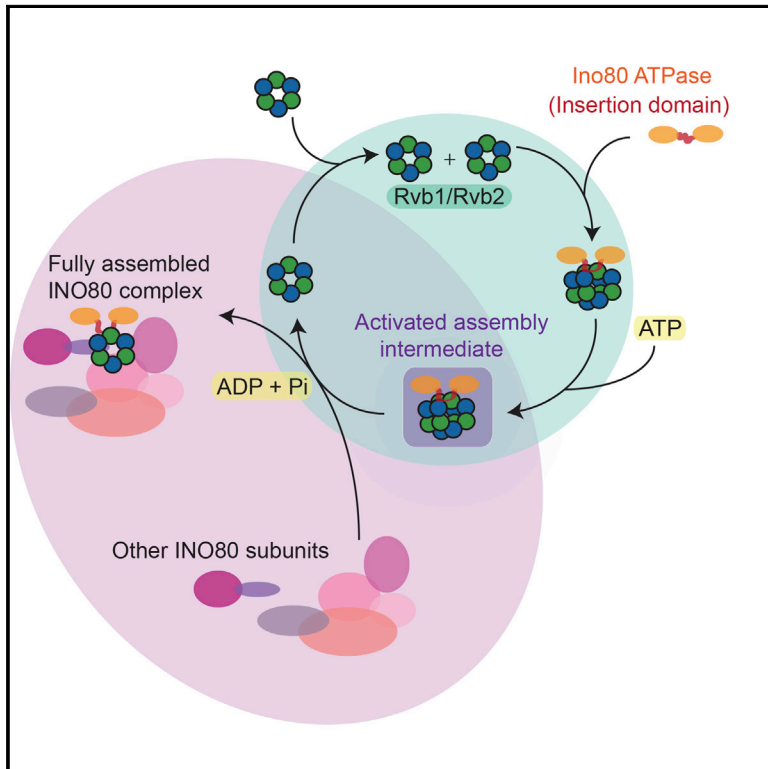


## Regulation of Rvb1/Rvb2 by a Domain within the INO80 Chromatin Remodeling Complex Implicates the Yeast Rvbs as Protein Assembly Chaperones

### Graphical Abstract



### Authors

Coral Y. Zhou, Caitlin I. Stoddard, Jonathan B. Johnston, ..., Alma L. Burlingame, Yifan Cheng, Geeta J. Narlikar

### Correspondence

geeta.narlikar@ucsf.edu

### In Brief

Rvb1 and Rvb2 (Rvbs) are AAA+ ATPases that have been hypothesized to assemble multi-subunit protein complexes, though this activity has not been experimentally demonstrated. Zhou et al. find that a domain within the chromatin remodeling Ino80 ATPase is a potent activator of Rvb1/Rvb2, creating a metastable dodecamer of Rvb/1Rvb2 that dissociates upon ATP addition.

### Highlights

- The insertion domain of the Ino80 ATPase (Ino80INS) activates yeast Rvb1/Rvb2
- Ino80INS activates Rvb1/Rvb2 by promoting dodecamerization of Rvb1/Rvb2
- Two copies of Ino80INS bind asymmetrically along the dodecameric interface of the Rvbs
- Addition of ATP to Rvb1/Rvb2/Ino80INS collapses the dodecamer into hexamers



# Regulation of Rvb1/Rvb2 by a Domain within the INO80 Chromatin Remodeling Complex Implicates the Yeast Rvbs as Protein Assembly Chaperones

Coral Y. Zhou,<sup>1,2</sup> Caitlin I. Stoddard,<sup>1,2</sup> Jonathan B. Johnston,<sup>3</sup> Michael J. Trnka,<sup>3</sup> Ignacia Echeverria,<sup>4</sup> Eugene Palovcak,<sup>1</sup> Andrej Sali,<sup>4,5,6</sup> Alma L. Burlingame,<sup>3</sup> Yifan Cheng,<sup>1,7</sup> and Geeta J. Narlikar<sup>1,8,\*</sup>

<sup>1</sup>Department of Biochemistry and Biophysics, University of California, San Francisco, San Francisco, CA 94158, USA

<sup>2</sup>Tetrad Graduate Program, University of California, San Francisco, San Francisco, CA 94158, USA

<sup>3</sup>Department of Pharmaceutical Chemistry, University of California, San Francisco, San Francisco, CA 94158, USA

<sup>4</sup>Department of Bioengineering and Therapeutic Sciences, University of California, San Francisco, San Francisco, CA 94158, USA

<sup>5</sup>Department of Pharmaceutical Chemistry, University of California, San Francisco, San Francisco, CA 94158, USA

<sup>6</sup>California Institute of Quantitative Biosciences, University of California, San Francisco, San Francisco, CA 94158, USA

<sup>7</sup>Howard Hughes Medical Institute, University of California, San Francisco, San Francisco, CA 94158, USA

<sup>8</sup>Lead Contact

\*Correspondence: [geeta.narlikar@ucsf.edu](mailto:geeta.narlikar@ucsf.edu)

<http://dx.doi.org/10.1016/j.celrep.2017.05.029>

## SUMMARY

The hexameric AAA+ ATPases Rvb1 and Rvb2 (Rvbs) are essential for diverse processes ranging from metabolic signaling to chromatin remodeling, but their functions are unknown. While originally thought to act as helicases, recent proposals suggest that Rvbs act as protein assembly chaperones. However, experimental evidence for chaperone-like behavior is lacking. Here, we identify a potent protein activator of the Rvbs, a domain in the Ino80 ATPase subunit of the INO80 chromatin-remodeling complex, termed Ino80INS. Ino80INS stimulates Rvbs' ATPase activity by 16-fold while concomitantly promoting their dodecamerization. Using mass spectrometry, cryo-EM, and integrative modeling, we find that Ino80INS binds asymmetrically along the dodecamerization interface, resulting in a conformationally flexible dodecamer that collapses into hexamers upon ATP addition. Our results demonstrate the chaperone-like potential of Rvb1/Rvb2 and suggest a model where binding of multiple clients such as Ino80 stimulates ATP-driven cycling between hexamers and dodecamers, providing iterative opportunities for correct subunit assembly.

## INTRODUCTION

AAA+ ATPases are a highly conserved family of molecular motors that use ATP binding and hydrolysis to drive a diverse set of structural rearrangements in their substrates (Singleton et al., 2007; White and Lauring, 2007). Rvb1 and Rvb2 (Rvbs) are two AAA+ ATPases from *S. cerevisiae* that are essential for many cellular processes, including transcription, cellular dif-

ferentiation, cell signaling, mitosis, small nucleolar ribonucleo-protein (snoRNP) assembly, and DNA-damage repair (Matias et al., 2015; Nano and Houry, 2013). Despite their extensive involvement in biology, the role of the Rvbs in these processes is unknown. Even the basic enzymatic function of these motors is poorly defined. While the Rvbs have ATPase activity (Gribun et al., 2008), there are competing models for how this activity contributes to the function of the Rvbs. Based on the structural similarity of the Rvbs to the bacterial helicase RuvAB, it was initially hypothesized that the Rvbs are DNA helicases. While a few groups have been able to detect DNA unwinding activity (Gribun et al., 2008; Kanemaki et al., 1999; Makino et al., 1999), other groups have reported a lack of such an activity (Ikura et al., 2000; Matias et al., 2006; Qiu et al., 1998). Recently, it has been proposed that the Rvbs act as protein assembly chaperones, based on the observation that the Rvbs co-purify with several multi-subunit protein complexes, including the R2TP complex, telomerase, snoRNP complexes, and chromatin remodeling complexes (Nano and Houry, 2013). However, no chaperone-like properties of the Rvbs have been experimentally demonstrated.

To investigate the possibility that the Rvbs act as assembly chaperones, we chose the yeast INO80 complex as a model system due to the wealth of biochemical and structural information available on this remodeling complex. We found that a small insertion within the Ino80 chromatin remodeling ATPase subunit of INO80 (Ino80INS) stimulates the ATPase activity of Rvb1/Rvb2 by 16-fold. To study how Ino80INS regulates Rvb structure and activity, we used a combination of crosslinking-mass spectrometry (MS), native MS, cryoelectron microscopy (cryo-EM), and integrative modeling approaches. Our results suggest a model in which (1) the activated dodecameric Rvb1/Rvb2/Ino80INS is poised to bring together several protein clients in close proximity, and (2) nucleotide binding and/or hydrolysis collapses the activated intermediate, helping assemble multi-subunit complexes containing a stably associated and less active Rvb1/Rvb2 hexamer.



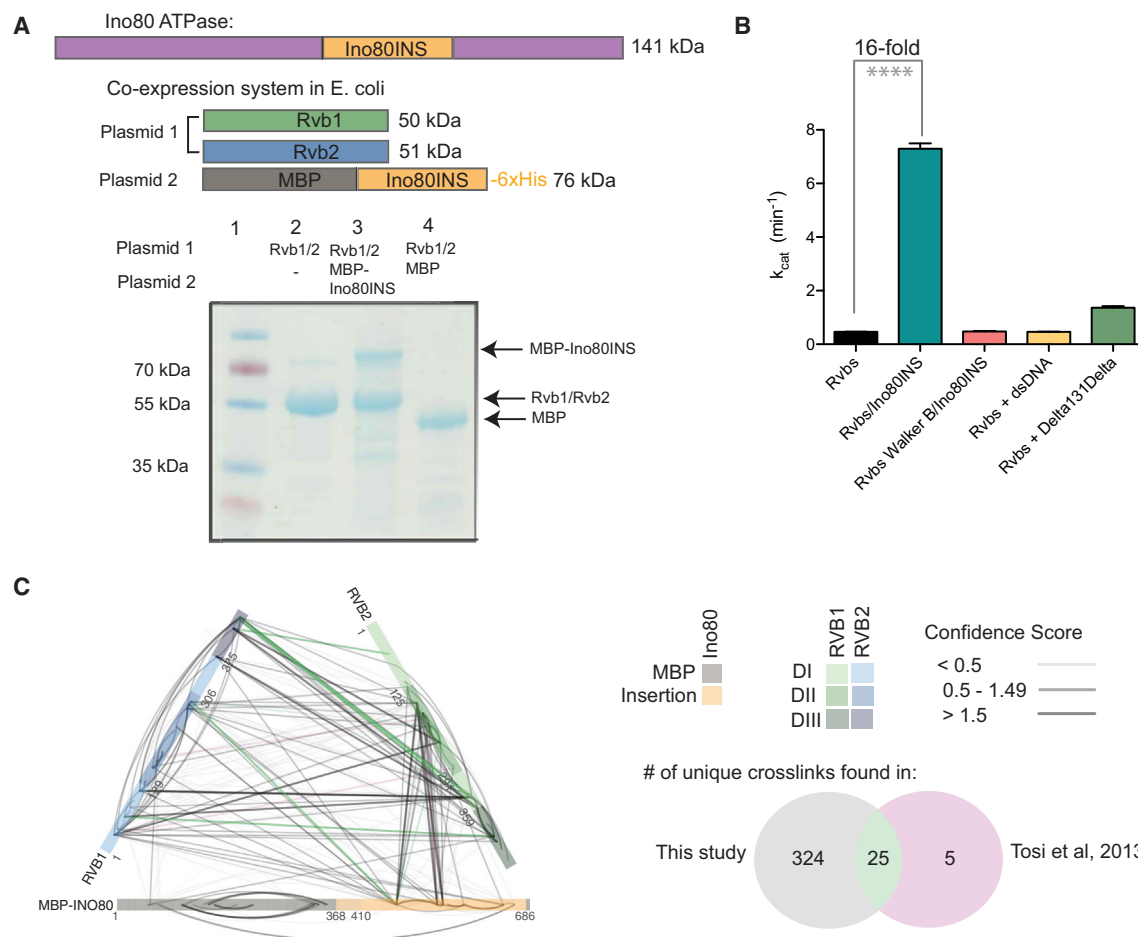


**Figure 1. The Insertion Domain of Ino80INS Is a Direct Interactor and Activator of Rvb1/Rvb2**

(A) Top: Sequence architecture of the Ino80 remodeling ATPase from yeast, with Ino80INS in yellow. Below this, the co-expression system for Rvb1/Rvb2/Ino80INS in *E. coli* is shown. Plasmid 1 contains Rvb1 and Rvb2. Plasmid 2 contains the Ino80 insertion (Ino80INS, residues 1,022–1,294) expressed as an MBP fusion and with a C-terminal His tag. Bottom: SDS-PAGE gel showing results of pull-down with co-expressed MBP-Ino80INS and Rvb1/Rvb2 (lane 3).

(B) Comparison of  $k_{cat}$  values for ATP hydrolysis by different Rvb1/Rvb2 and Rvb1/Rvb2/Ino80INS complexes. Stimulation of 5  $\mu$ M Rvbs with either 25  $\mu$ M double-stranded DNA (dsDNA) or MBP- $\Delta$ 131 $\Delta$  is indicated in yellow and green, respectively. Error bars represent the mean  $\pm$  SEM of three replicates. \*\*\*\* $p < 0.0001$ .

(C) XL-MS data for the Rvb1/Rvb2/Ino80INS complex. Rvb1 (green) and Rvb2 (blue) are shown with different shades representing DI, DII, and DIII. Crosslinks found only in our dataset, in only the native INO80 complex (Tosi et al., 2013), or in both datasets are shown in gray, pink, and green, respectively (see Venn diagram). The confidence of the MS identification (SVM score) is represented by the thickness and transparency of the lines.

See also Figure S1 and Table S1.

## RESULTS

### The Insertion Domain of the Ino80 ATPase Is a Potent Activator of Rvb1/Rvb2

An early study showed that the ATP hydrolysis activity of Rvb2 is required for the formation of active INO80 complexes in yeast (Jónsson et al., 2004). Recently, it was shown that a small insertion within the Ino80 ATPase subunit (Ino80INS; Figure 1A, top) is required for association with the Rvbs and other subunits of the complex that are critical for activity (Chen et al., 2013). These results suggested that Ino80INS is used by the Rvbs as a scaffold for assembling an active INO80 complex. To test this possibility, we asked whether Ino80INS, on its own, could directly interact

with the Rvb1/Rvb2 complex and whether or not this interaction influences the ATPase activity of the Rvbs.

We co-expressed untagged Rvb1 and Rvb2 along with a His-tagged, MBP (maltose-binding protein)-Ino80INS fusion in *Escherichia coli*. These three proteins form a stable complex that purified as a single peak over a size exclusion column (Figure 1A). Efforts to purify the complex without an MBP tag on Ino80INS, or MBP-Ino80INS alone, were unsuccessful, suggesting that Ino80INS is inherently unstable but can be stabilized via interactions with Rvb1 and Rvb2. Next, we tested whether the activity of the Rvbs is affected by Ino80INS and found that Rvb1/Rvb2/Ino80INS has a 16-fold greater catalytic rate constant,  $k_{cat}$ , for ATP hydrolysis than Rvbs alone. In contrast, an

excess of DNA did not stimulate the Rvbs' ATPase activity, consistent with previously published results with human Rvb1/Rvb2 (Puri et al., 2007). Interestingly, the partially unfolded region of staphylococcal nuclease  $\Delta 131\Delta$ , routinely used as a model substrate for the chaperone Hsp90 (Street et al., 2011), modestly stimulated the ATPase activity of the Rvbs (2- to 3-fold; Figure 1B). This result further suggests that protein, not DNA, is the biologically relevant substrate for yeast Rvb1/Rvb2.

We next used crosslinking MS (XL-MS) (Leitner et al., 2016) to investigate residue-level interactions between the Rvbs and Ino80INS. From two separate XL-MS experiments with the Rvb1/Rvb2/Ino80INS (Figure 1C) and the Rvb1/Rvb2 alone (Figure S1A), we identified 519 unique crosslinked residue pairs ("crosslinks") at a false discovery rate of 1.7% (Figure S1B; Table S1). Strikingly, a majority of the high-confidence crosslinks containing Ino80INS mapped to the DII regions of Rvb1 and Rvb2 (Figure 1C). The DII domains are of particular interest, due to their role in regulating the activity and oligomeric state of the Rvbs (Gorynia et al., 2011; Niewiarowski et al., 2010). Very few residues from the Rvbs crosslinked to MBP (Figure 1C), confirming that the complex is predominantly stabilized by direct interactions between the DII regions of Rvb1/Rvb2 and Ino80INS. Also, our data recapitulate over 80% of the interactions found in a crosslinking study of the complete yeast INO80 complex (Tosi et al., 2013), suggesting that the Rvb1/Rvb2/Ino80INS subcomplex maintains the same interactions as seen within the native INO80 complex.

### The Ino80 Insertion Promotes Dodecamerization of Rvb1/Rvb2

Rvbs are predominantly hexameric, but a small population of naturally occurring dodecamers has also been reported (Jeganathan et al., 2015). Our observation that Ino80INS binds predominantly to the DII regions of the Rvbs raised the possibility that Ino80INS may activate the Rvbs' ATPase activity by altering the oligomeric state of Rvb1/Rvb2. To investigate this possibility, we used size exclusion chromatography-multi-angle light scattering (SEC-MALS) to determine the molecular weight of Rvb1/Rvb2/Ino80INS. We found that the complex has a molecular weight that is most consistent with that of a dodecamer of Rvb1/Rvb2 bound to at least two copies of the Ino80 insertion (Figure 2A). In contrast, Rvb1/Rvb2 alone gave a molecular weight most consistent with that of hexamers.

To further analyze the distribution of species in the Rvb1/Rvb2/Ino80INS sample, we turned to native MS. Using this technique (Rose et al., 2012), we found two distinct charge envelopes with masses consistent with either two or three copies of Ino80INS bound to a single Rvb1/Rvb2 dodecamer (Figures 2B, S2A, and S2B; Table S2). Along with the SEC-MALS results, these data suggest that more than one Ino80INS can bind to a single dodecamer of Rvb1/Rvb2. In addition to the dodecamer, we also observed a small population of Rvb1/Rvb2 hexamer (Species 1 in Figures 2B and S2B; Table S2) and Rvb1/Rvb2 hexamer bound to a single MBP-Ino80INS (Species 2 in Figures 2B and S2B; Table S2). Intriguingly, addition of ATP-Mg<sup>2+</sup> to the Rvb1/Rvb2/Ino80INS complex caused the dodecameric species to convert to a hexameric species (Figure 2C). We also observed dissociation into hexamers by negative-stain EM, as barrel-

shaped Rvb1/Rvb2 dodecamers fall apart to ring-shaped hexamers upon addition of ATP-Mg<sup>2+</sup> (Figure S2C). These results suggest that destabilization of the Rvb1/Rvb2/Ino80INS dodecamer is coupled to the nucleotide state of the Rvbs.

### Nucleotide State Drives the Switch between Hexameric and Dodecameric Forms of Rvb1/Rvb2

Our observation that the Rvb1/Rvb2/Ino80INS complex collapses in an ATP-dependent manner raised the possibility that the transition between dodecamer and hexamer is a core activity of the Rvbs and may be related to the Rvbs' ability to function as a chaperone. To further investigate how the oligomeric state of the Rvbs alone is regulated by ATP state, we used native MS to analyze the relative populations of oligomers of Rvb1/Rvb2 in different nucleotide states. The high mass resolution of this method also allowed us to more accurately determine subunit stoichiometry and the nucleotide-binding state of each oligomer. Untagged yeast Rvb1/Rvb2 ionized as hexamers with a mass that is most consistent with a 3:3 stoichiometry of Rvb1: Rvb2 (Figures 3A, S3A, and S3B; Table S3), in contrast to a 4:2 stoichiometry reported for human Rvbs (Niewiarowski et al., 2010). Intact denatured MS on the same sample confirmed the 3:3 stoichiometry (Figure S3C).

We next addressed how the Rvb1/Rvb2 dodecamer might be affected by nucleotide state. This experiment could not be performed with untagged Rvb1/Rvb2, as the complex is predominantly a hexamer at concentrations compatible with native MS (1  $\mu$ M) with and without nucleotide (Figures 3A and S3D). Previous work with yeast Rvb1/Rvb2 showed that an N-terminal His-tag promotes dodecamerization, providing a means to study the dodecameric state by native MS (Cheung et al., 2010; Jeganathan et al., 2015). As expected, His-tagged Rvbs ionized as a dodecamer (Figure 3B). When an excess of ATP-Mg<sup>2+</sup> was added, a small proportion (14%) of the dodecamer dissociated into hexamers (Figure 3C; Table S4), consistent with our observation for the Rvb1/Rvb2/Ino80INS complex (Figure 2C).

To test which stage(s) of the ATPase cycle affects oligomerization, we used the non-hydrolyzable ATP analogs AMP-PNP and ATP- $\gamma$ -S to mimic the ATP-bound state and ADP to mimic the post-hydrolysis state. Surprisingly, AMP-PNP, ATP- $\gamma$ -S, and ADP all substantially increased the proportion of the hexameric state (Figures 3D–3E and S3E). Importantly, this increase was greater than what was observed with ATP (Figures 3C versus 3D and 3E; Table S4). The quantitative difference in the effects we observed with AMP-PNP versus ATP does not appear to be due to differences in affinity of the nucleotide for Rvb1/Rvb2, as similar amounts of nucleotide loading were observed for both ATP-Mg<sup>2+</sup> and AMP-PNP-Mg<sup>2+</sup> (Table S4). To further investigate the role of nucleotide binding versus hydrolysis, we mutated the Walker B motifs of Rvb1 and His-Rvb2, which diminished ATP hydrolysis by >20-fold (Figure S3F). Compared to wild-type Rvb1/his-Rvb2, the population of hexamers in the Walker B Rvb1 Walker B/his-Rvb2 Walker B mutants increased dramatically, from 0% to 84%, and the addition of ATP gave similar results (Figures 3F and S3I; Table S4). These results suggest a model in which nucleotide binding promotes a conformation of the Rvbs that stabilizes the hexameric state, while a different intermediate in the ATP hydrolysis reaction stabilizes a conformation that promotes formation of a metastable dodecamer (Figure 3G).

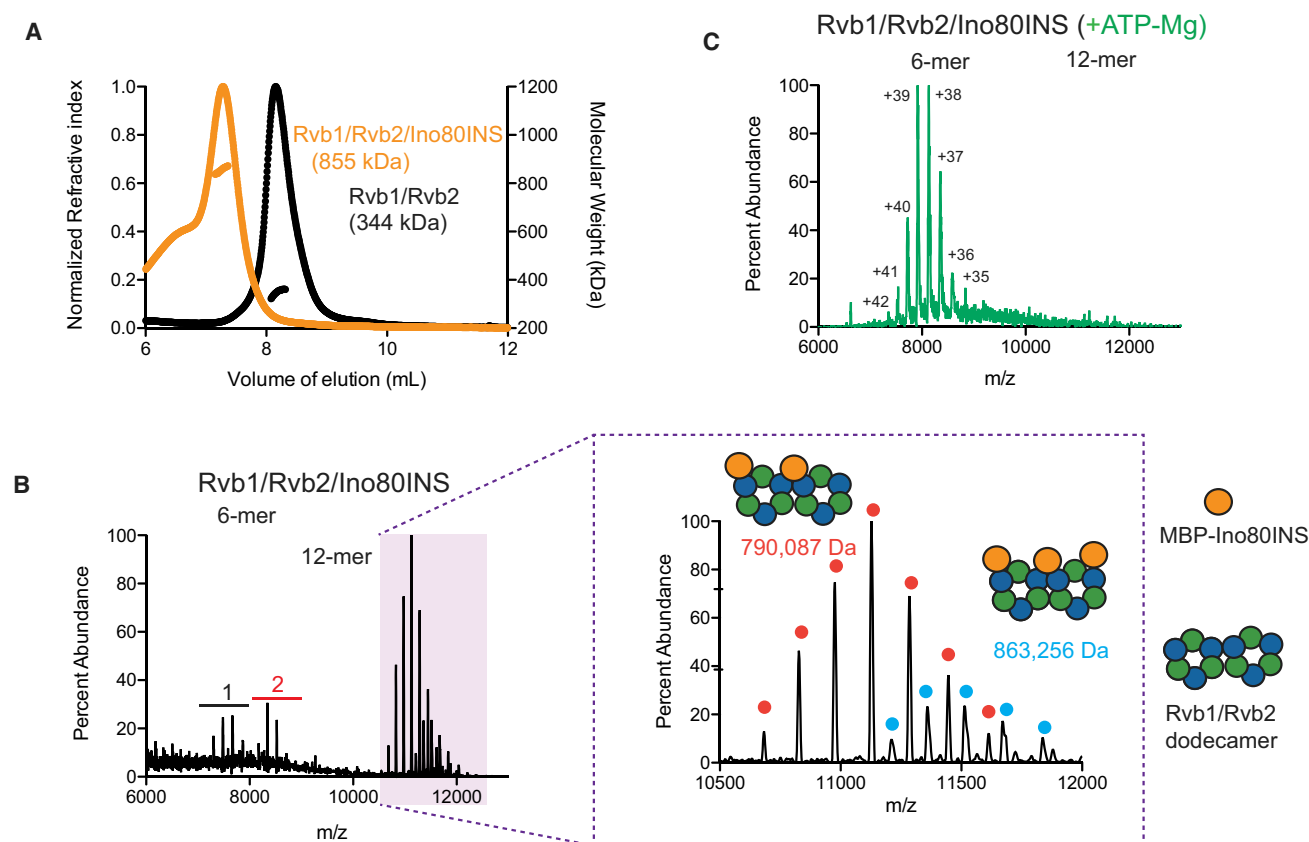


**Figure 2. The Ino80 Insertion Promotes Dodecamerization of Rvb1/Rvb2**

(A) SEC-MALS of Rvb1/Rvb2/Ino80INS complexes. Normalized refractive index (left y axis) and molecular weight of the major peak (right y axis) are plotted against the volume of elution. For each experiment, either 10  $\mu$ M Rvb1/Rvb2/Ino80INS (orange) or 30  $\mu$ M Rvb1/Rvb2 (black) was injected. The molecular weights shown in corresponding colors are an average of the calculated molecular-weight values across the main peak.

(B) Left: raw spectrum of Rvb1/Rvb2/Ino80 complexes using native MS. Charge envelopes for the hexameric species are shown in black (1) and red (2). Right: an expanded view of the charge envelopes representing the two dodecameric species. Cartoons representing the MBP-Ino80INS and Rvb1/Rvb2 illustrate the predicted stoichiometries represented by the two charge envelopes.

(C) Raw spectrum of 1  $\mu$ M Rvb1/Rvb2/Ino80INS complexes with 20  $\mu$ M ATP-Mg added, by native MS.

See also [Figure S2](#) and [Table S2](#).

For these studies, it is important to note that the His-tag is not present on the Rvbs in vivo, so the biological significance of the His-tagged dodecameric species is unclear. However, since the basic observation we derive from the His-tagged construct—namely, disassembly into hexamers in the presence of ATP—is recapitulated in the context of untagged Rvbs bound to a native protein activator (Ino80INS) we suggest that the behavior of the His-tagged complex captures some of the core features of a native Rvb complex.

#### ATPase Activity of the Rvb1/Rvb2 Complex Is Enhanced by Dodecamerization

We previously observed that the stimulation of Rvbs by Ino80INS is concurrent with the dodecamerization of Rvb1/Rvb2. We next asked whether this correlation exists in a context outside of Ino80INS. Similar to the N-terminal His-tag, replacing the DII domain with a flexible linker also increases dodecamerization of Rvbs, but there is conflicting evidence for how these mutants affect the Rvbs' ATPase activity in the yeast system ([Gorynia](#)

[et al., 2011](#); [Jeganathan et al., 2015](#); [Niewiarowski et al., 2010](#)). When we deleted the DII domains in Rvb1 and Rvb2, we found that this Rvb1 $\Delta$ DII/Rvb2 $\Delta$ DII complex has a molecular weight (341 kDa) that is in between what is expected for a dodecamer (474 kDa) and a hexamer (237 kDa) by SEC-MALS ([Figure 4A](#); [Table S5](#)). We reasoned that the intermediate molecular weight could reflect either a rapidly exchanging mixture of hexamer and dodecamer or a homogeneous population of an oligomeric state between a dodecamer and a hexamer ([Table S5](#)). Increasing the concentration of Rvb1 $\Delta$ DII/Rvb2 $\Delta$ DII from 10  $\mu$ M to 30  $\mu$ M resulted in a 437-kDa complex that is approximately the expected molecular weight of a dodecamer ([Figure S4A](#); [Table S5](#)). Native MS with 1  $\mu$ M Rvb1 $\Delta$ DII/Rvb2 $\Delta$ DII indicated predominantly hexamers with a small (3%) population of dodecamer ([Figure S4C](#)), consistent with a concentration-dependent oligomerization of Rvb1 $\Delta$ DII/Rvb2 $\Delta$ DII. In contrast, wild-type Rvb1/Rvb2 remained hexameric at 80  $\mu$ M ([Figure S4B](#)).

We next compared the maximal ATPase activity ( $k_{cat}$ ) of the different Rvb1/Rvb2 mutants. We found that adding a His-tag

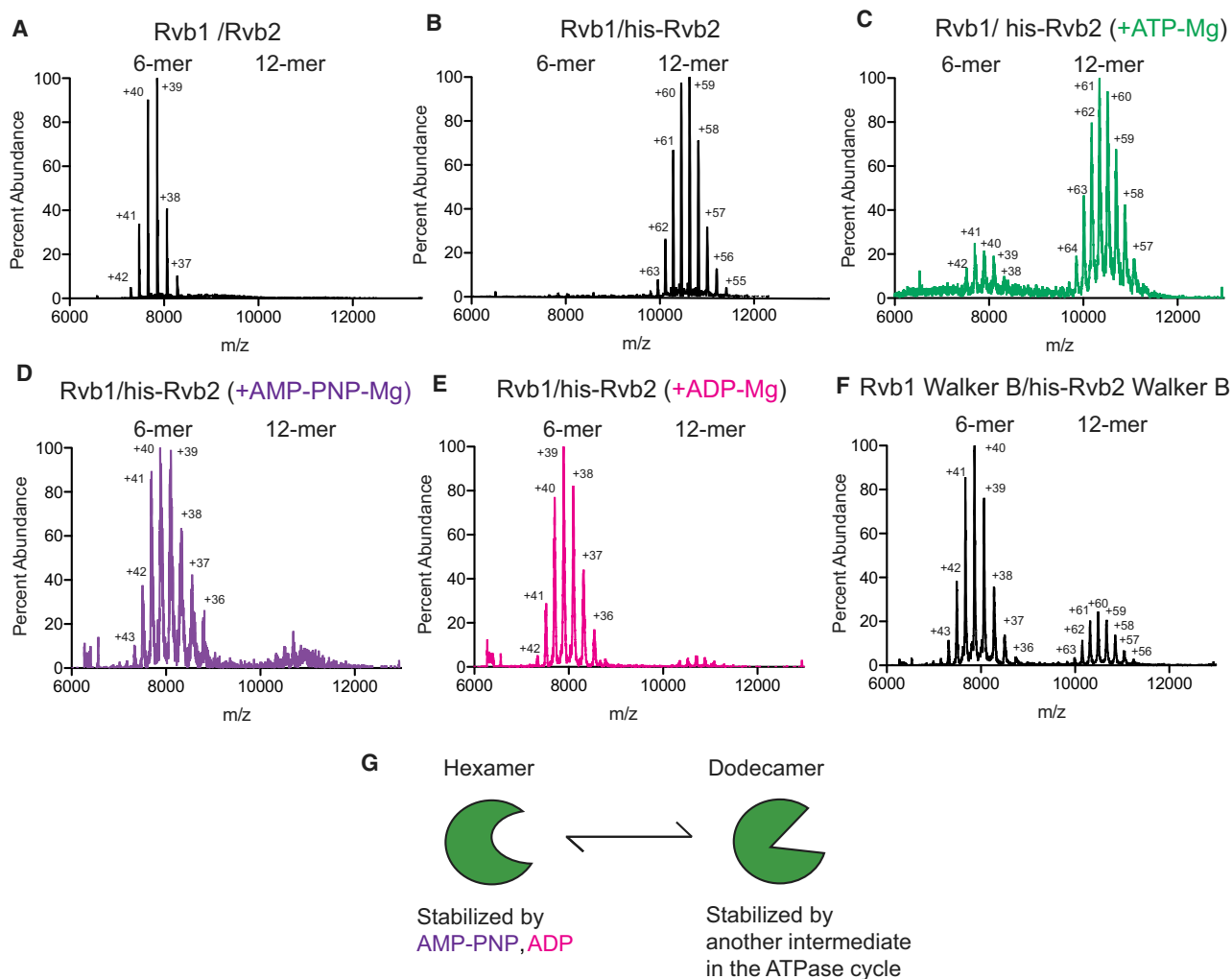


**Figure 3. Nucleotide State Drives the Switch between Hexameric and Dodecameric Forms of the Rvb1/Rvb2 Complex**

(A) Raw spectrum of 1  $\mu$ M untagged Rvb1/Rvb2 by native MS. m/z, mass-to-charge ratio.  
 (B) Raw spectrum of 1  $\mu$ M Rvb1/His-Rvb2.  
 (C) Raw spectrum of 1  $\mu$ M Rvb1/Rvb2-His tag after addition of 20  $\mu$ M ATP-Mg.  
 (D) Raw spectrum of 1  $\mu$ M Rvb1/Rvb2-His tag after addition of 20  $\mu$ M AMP-PNP-Mg.  
 (E) Raw spectrum of 1  $\mu$ M Rvb1/Rvb2-His tag after addition of 20  $\mu$ M ADP-Mg.  
 (F) Raw spectrum of 1  $\mu$ M His-tagged Walker B mutants of Rvb1 (D311N) and Rvb2 (D296N).  
 (G) Model for how hexameric and dodecameric states of Rvbs are regulated by nucleotide state.  
 See also [Figure S3](#) and [Tables S3](#) and [S4](#).

to Rvb2 increased the  $k_{cat}$  for ATP hydrolysis only 2-fold, while deleting the DII domains of Rvb1 and Rvb2 increased the specific activity by 7-fold ([Figure 4B](#)). Taken together with the data in [Figure 2](#), these data suggest that the ATPase cycle of Rvb1/Rvb2 drives a constant inter-conversion between hexamers and dodecamers, resulting in a defined steady-state distribution of the two oligomeric states with different specific activities ([Figure 4C](#)). The regulation of the Rvbs' activity by Ino80INS serves as a natural extension of this model, as binding of Ino80INS to the DII domains of the Rvbs promotes an activated, metastable dodecamer that easily dissociates into hexamers upon addition of ATP.

### Cryo-EM Reconstruction of the Rvb1/Rvb2/Ino80INS Complex Suggests a High Degree of Conformational Flexibility

We were next curious about the structural basis of how Ino80INS engages the DII domains of Rvb1/Rvb2 to create a metastable dodecamer. Previous studies of Rvb1/Rvb2 have reported a high degree of conformational flexibility within the DII regions ([Ewens et al., 2016](#); [Gorynia et al., 2011](#); [Jeganathan et al., 2015](#); [López-Perrote et al., 2012](#); [Petukhov et al., 2012](#)), which appear to form the dodecameric interface. A crystal structure of the Rvb1/Rvb2 complex from the thermophilic fungus *Chaetomium thermophilum* ([Lakomek et al., 2015](#)) shows one

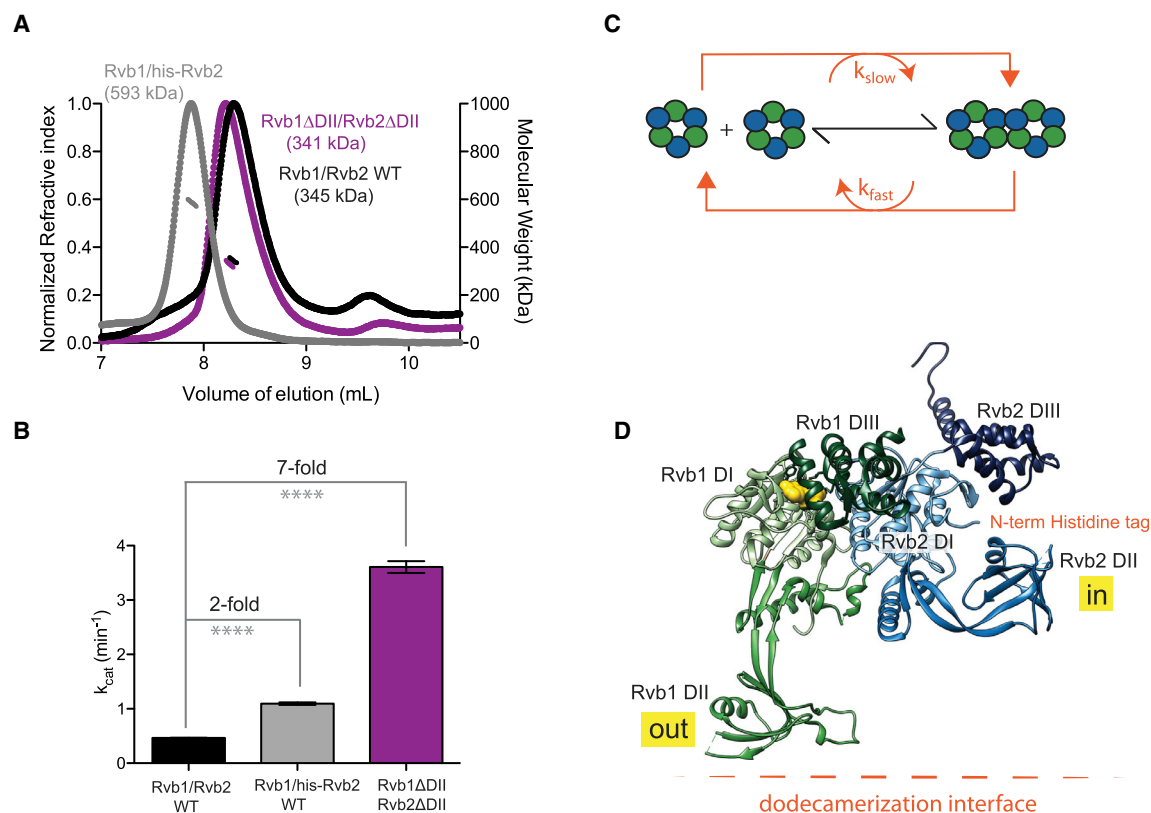


**Figure 4. The ATPase Activity of the Rvb1/Rvb2 Complex Is Enhanced by Dodecamerization**

(A) SEC-MALS of different Rvb1/Rvb2 complexes. Normalized refractive index (left y axis) and molecular weight of the major peak (right y axis) are plotted against the volume of elution. 10  $\mu$ M of Rvb1/Rvb2 (black), Rvb1/Rvb2-his (gray), or Rvb1 $\Delta$ DII, Rvb2 $\Delta$ DII (purple) was injected. The molecular weights shown in corresponding colors are an average of the calculated molecular-weight values across the main peak.

(B)  $k_{cat}$  for ATP hydrolysis activity for different Rvb1/Rvb2 complexes. Experiments were performed using 10 mM Rvbs and saturating ATP. Error bars represent the mean  $\pm$  SEM of three replicates. \*\*\*\* $p < 0.0001$ . WT, wild-type.

(C) Model for how the Rvb1/Rvb2 oligomeric state is coupled to the ATPase cycle. Rvb1/Rvb2 complexes exist at equilibrium between hexamer and dodecamer (black arrows). In the presence of nucleotide, Rvb1/Rvb2 complexes are constantly interchanging between the two oligomeric states (orange arrows), creating a steady-state distribution of the hexamer and dodecamer, where hexamers hydrolyze ATP more slowly ( $k_{slow}$ ) than dodecamers ( $k_{fast}$ ).

(D) Top: domain architecture of Rvb1 and Rvb2 from *S. cerevisiae*. Domains of Rvb1 are colored as different shades of green, and domains of Rvb2 are colored as different shades of blue. Bottom: model of Rvb1 (bound to ATP) and Rvb2 (apo) adapted from the crystal structure of Rvb1/Rvb2 complex from *Chaetomium thermophilum* (Lakomek et al., 2015; PDB: 4WVY). Domains I and III contain the catalytic residues, while domain II folds as a separate module in either the “in” or the “out” state. The location of the N-terminal His tag, which does not appear in the density, is shown in orange, and ATP is shown in yellow.

See also Figure S4 and Table S5.

possible arrangement of the Rvb1 and Rvb2 DII domains: the Rvb2 DII domains fold back toward the hexameric ring (“in” state), and the Rvb1 DII domains extend toward a second hexamer (“out” state) (Figure 4D). Therefore, we imagined two extreme models for how Ino80INS binding may alter the structure of the Rvbs: (1) Ino80INS “locks” the conformationally flexible dodecameric interface into one predominant conformation, or (2) Ino80INS binds in a way that maintains the natural conformational flexibility of the DII domains.

To test these hypotheses, we determined the cryo-EM map of the Rvb1/Rvb2/Ino80INS complex at  $\sim$ 12.0-Å resolution (Figures 5B and S5B). Both raw images and 2D class averages show a distinct barrel shape created by the two hexameric rings flanking the DII domains of the Rvbs (Figures 5A and S5A). We also observed both bent and straight conformations of the Rvb1/Rvb2/Ino80INS dodecamer in our 2D classes (Figure 5A). These

features are similar to those reported in a recently published cryo-EM structure of Rvb1/Rvb2 dodecamers without an activator bound (Ewens et al., 2016; Silva-Martin et al., 2016), suggesting that Ino80INS binding does not substantially diminish the natural dynamics of the Rvbs.

To further investigate the extent of the conformational dynamics in the Rvb1/Rvb2/Ino80INS complex, all particles used for 2D classification were also used for 3D refinement to generate a consensus cryo-EM map (Figure 5B), with no imposed symmetry. Interestingly, the bent feature observed in the 2D classes is retained in the consensus map, suggesting that it is a common feature of most of the particles. To find higher resolution subpopulations of the dataset, we further subclassified particles to generate 12 different 3D classes (Figure 5C). Each class contained a similar number of particles and had resolutions that were similar to one another and to

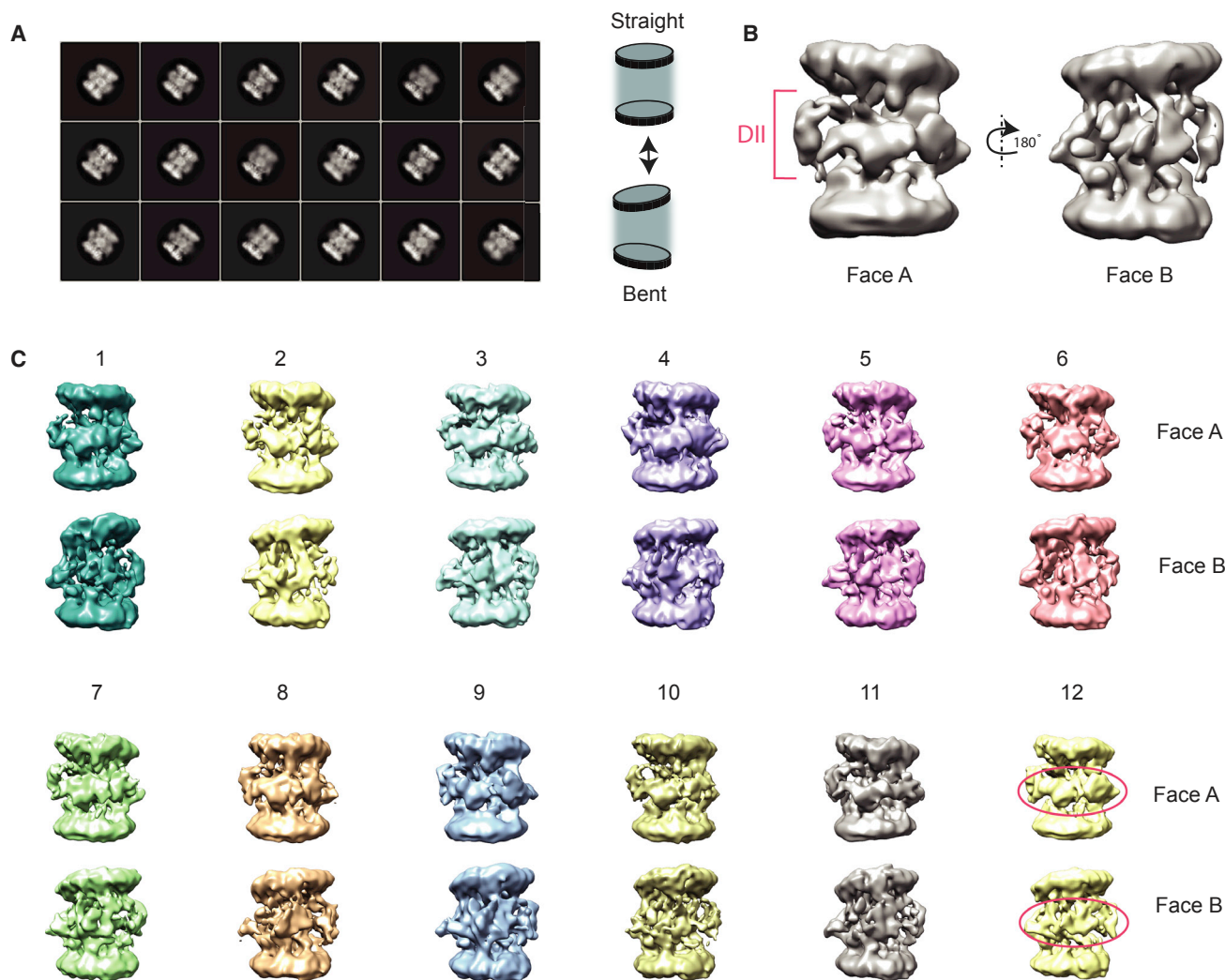


**Figure 5. Cryo-EM of the Rvb1/Rvb2/Ino80INS Complex Reveals Conformational Heterogeneity**

(A) Left: side views of reference-free 2D class averages of Rvb1/Rvb2/Ino80INS particles. Right: scheme displaying “bent” and “straight” features of the Rvb1/Rvb2/Ino80INS dodecamer.

(B) Rvb1/Rvb2/Ino80INS consensus model generated by refinement of all 366,000 particles used for 2D classification in (A).

(C) Twelve 3D classes representing all of the particles used for the consensus structure in (B). The top and bottom rows of each class represent two opposite faces of the dodecamer. Each class contains approximately 30,000 particles.

See also Figure S5.

that for the consensus map. Despite many rounds of further subclassification, we were unable to achieve higher resolution, implying a high degree of conformational heterogeneity in the system. This conformational heterogeneity is most prominent in the densities surrounding the DII domains, as well as in the degree of tilt observed between the two hexameric rings (Figure 5C). In addition to the conformational heterogeneity, a second general feature of the Rvb1/Rvb2/Ino80INS system is its asymmetry at the dodecameric interface. In both the consensus map and each of the 12 subclasses, one face of the dodecamer consistently shows bulkier density than the opposite face of the dodecamer (Figures 5B and 5C, Face A versus Face B).

#### Ino80INSs Bind Asymmetrically on the Rvb1/Rvb2 Dodecamer

To obtain more insight into the conformational flexibility and asymmetry of the Rvb1/Rvb2/Ino80INS complex, we mapped all unique Rvb-Rvb crosslinks observed in the Rvb1/Rvb2/Ino80INS complex onto a comparative structural model of the yeast Rvb1/Rvb2 dodecamer. We created this model based on sequence identity between the *S. cerevisiae* Rvb1 and Rvb2 subunits and the *S. thermophilus* structure of the Rvb1/Rvb2 dodecamer (Lakomek et al., 2015). Strikingly, this mapping revealed that only 58% of the unique 226 Rvb-Rvb crosslinks are satisfied (Figure S7A). It is unlikely that the low percentage of satisfied crosslinks is due to inaccurate spectral assignments,

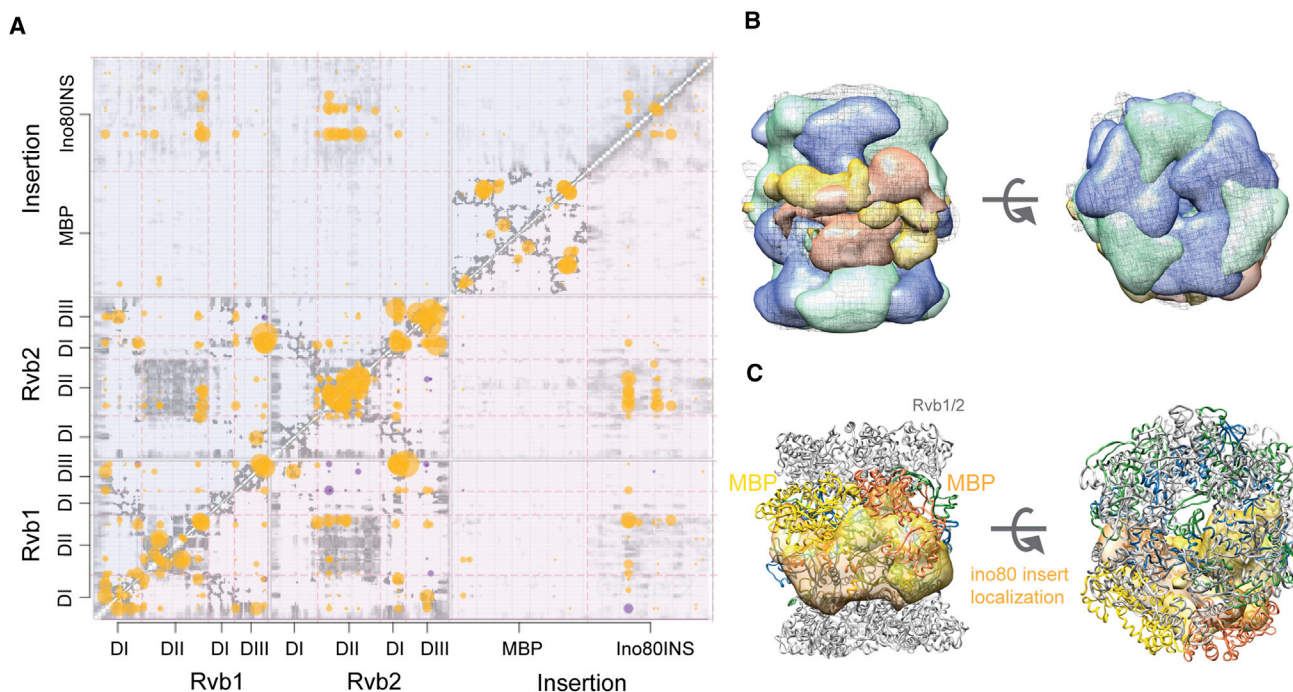


**Figure 6. Ino80INS Binds to Rvb1/Rvb2 Dodecamer Asymmetrically**

(A) Characterization of Clusters 1 (top half, shaded light blue) and 2 (bottom half, shaded light red). The gray bins indicate pairs of proximal beads representing the model, with the intensity of gray proportional to the fraction of models in the cluster whose distance is closer than the cutoff of 12 Å. The yellow circles correspond to the crosslinks satisfied by at least one model in a cluster, with the size of the circle proportional to the spectral count. The purple circles indicate crosslinks that are not satisfied by any model in the cluster.

(B) Side and top views of the localization density maps for Rvb1 (green), Rvb2 (blue), and MBP-Ino80INS (orange and yellow) calculated for cluster 1 (thresholded at 0.15). The gray mesh shows the consensus EM density map.

(C) Top and side views of a representative model from cluster 1. The distributions of the two copies of Ino80INS are shown by their localization densities (indicated in orange and yellow).

See also [Figures S6](#) and [S7](#) and [Table S6](#).

given the low false discovery rate (FDR) of our crosslinking experiment (less than 2%; [Figure S3B](#)). It is also unlikely that our comparative model of the Rvb1/Rvb2 dodecamer is insufficiently accurate to explain the XL violations, given the high sequence similarity between the *S. cerevisiae* and *S. thermophilus* Rvbs (73% for Rvb1 and 72% for Rvb2) and the high structural conservation in this family ([Iyer et al., 2004](#)). Thus, the high proportion of crosslinks violated by the model is likely due to the additional conformations that the Rvb1/Rvb2/Ino80INS complex can adopt beyond the one exhibited in the comparative model of the Rvb1/Rvb2 dodecamer.

To better characterize this conformational heterogeneity, we applied an integrative structure determination approach based on all information available for the Rvb1/Rvb2/Ino80INS complex, including the XL-MS dataset ([Figure 3C](#); [Table S4](#)), the consensus cryo-EM map ([Figure 5B](#)), the comparative model of the Rvb1/Rvb2 dodecamer, the crystal structure of MBP ([Kim, 2013](#)), and the predicted secondary structure of Ino80INS ([Figure S6](#); [Table S6](#)). The resulting integrative models are expected to be more accurate and precise than models based on a subset of data ([Alber et al., 2007](#); [Robinson et al., 2015](#); [Ruszel et al., 2012](#); [Shi et al., 2014](#)). We imposed a stoichiometry of two copies of Ino80INS bound to one Rvb1/Rvb2 dodecamer

based on the major species found by native MS ([Figure 2C](#)). The ensemble of models, consistent with input information, was computed by satisfying spatial restraints implied by the data, allowing us to quantify the structural heterogeneity and asymmetry observed in the cryo-EM data as well as to predict the binding site of Ino80INS.

The ensemble contains three clusters of models, each of which represent possible conformations of the Rvb1/Rvb2/Ino80INS dodecamer. For cluster 1, the precision (average pairwise root-mean-square deviation [RMSD] of the models in the cluster) is 25 Å, and the precisions of the Rvb1/Rvb2 dodecamer and Ino80INS in particular are 15.8 and 39.3 Å, respectively. These values represent the average fluctuations of the individual residues or beads in 3D space across the ensemble of solutions. The precisions of the other two clusters are comparable ([Table S6](#)). Each cluster of models satisfies the XLs approximately within the expected tolerance (>90%) ([Figure 6A](#); [Table S6](#)), and 98% of all crosslinks are satisfied by at least one structure in the three clusters. The remaining 2% unsatisfied crosslinks are likely explained by the 2% false-positive rate of crosslinking, sample heterogeneity, insufficient conformational sampling, and coarse-grained representation of the modeled components. Each cluster matches the EM density map, as demonstrated

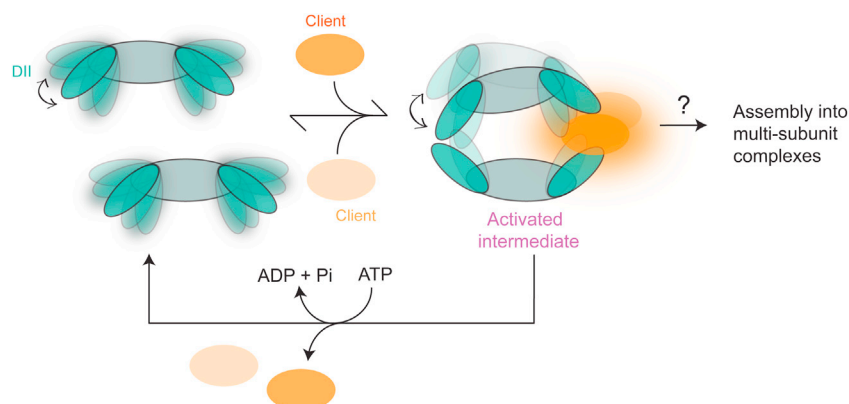


**Figure 7. Model for Activation of Rvb1/Rvb2 by Client Proteins**

Binding of client proteins to DII domains of Rvb1/Rvb2 promotes the dodecameric state by stabilizing the flexible DII regions that constitute the dodecamerization interface. Two clients bind asymmetrically to the dodecamer, creating an activated intermediate that is highly competent for ATP hydrolysis. Addition of ATP causes the dodecamer to fall apart, allowing the two client proteins to be assembled into a multi-subunit complex. Meanwhile, Rvb1/Rvb2 hexamers are recycled and poised to repeat the assembly reaction.

by the overlaps of the cluster localization density maps with the consensus cryo-EM density map when all maps are contoured to match their volumes (Figure 6B; Table S6). A localization density map for a set of models is defined as the probability of observing a model component at any point in space (Robinson et al., 2015). Because each cluster satisfies the crosslinks and EM map comparably well, and each cluster contains a comparable number of solutions, it is likely that the localization density maps represent the underlying conformational heterogeneity in the sample rather than a lack of information used for modeling.

In all clusters, Ino80INS binds to the central region of the barrel, contacting the DII domains (Figures 6A and S7C). Furthermore, the two Ino80INS domains bind asymmetrically on the Rvb1/Rvb2 dodecamer, contacting the same side of the barrel. Examination of the MBP crosslinks shows that some crosslinks are necessarily inter-molecular (Figure S7B), suggesting that the two MBP domains are close to each other. Due to the proximity of the Ino80 and MBP domains in the linear sequence, this observation further supports a model of asymmetric binding of the two copies of INO80INS to the Rvbs dodecamer.

## DISCUSSION

In addition to the INO80 complex, Rvb1 and Rvb2 have been found to associate with a number of multi-subunit complexes, including snoRNP complexes (McKeegan et al., 2009), phosphatidylinositol 3-kinase-related protein kinase (PIKK) signaling complexes (Izumi et al., 2010), and telomerase (Venteicher et al., 2008), leading to the hypothesis that the Rvbs may act as chaperones for assembling and/or remodeling these complexes (Nano and Houry, 2013). Based on our data and prior work, we propose the following model for how the Rvbs may help assemble multi-subunit complexes such as INO80 (Figure 7). In this model, nucleotide binding is coupled to a conformation of the Rvb that is autoinhibitory for ATP hydrolysis and incompatible with dodecamerization, while ATP hydrolysis (either the transition state or the ADP-P<sub>i</sub> product state) is coupled to a conformation of the Rvb that promotes dodecamerization (Figure 3G). Binding of clients such as Ino80INS then drives the Rvbs into the more active dodecameric state, yet one that is metastable and is more likely to dissociate into hexamers (Figure 2). Thus, a window of opportunity is created for other client

proteins to bind to adjacent DII domains of the Rvb1/Rvb2 complex. We speculate that the Rvb1/Rvb2 dodecamer is able to “sense” co-localization of multiple client proteins by coupling the association of these proteins to nucleotide-driven dissociation of the dodecamer into hexamers. This model is consistent with our observation that two copies of Ino80INS can bind asymmetrically to one side of the Rvb1/Rvb2 dodecamer (Figure 6), which, we speculate, reflects the ability of the Rvb1/Rvb2 dodecamer to bind to multiple different client proteins in vivo.

A major feature of our model is that binding of a client protein such as Ino80INS promotes the formation of a metastable dodecamer that is prone to collapsing into hexamers upon nucleotide binding. Our cryo-EM and integrative modeling data provide structural insight into how such a metastable dodecamer is created, as the dodecameric interface is highly flexible and dynamic (Figures 5 and 6). The ability of ATP to further destabilize this interface is consistent with recently published cryo-EM structures of the Rvb1/Rvb2 dodecamers alone, which suggest that the addition of nucleotide causes a significant reconfiguration of the DII domains, resulting in a shift in the relative orientations of the two hexameric rings (Ewens et al., 2016). Therefore, we speculate that creation of a metastable dodecamer through reconfiguration of the DII domains is important for both the ATP-driven cycling between hexamers and dodecamers and the chaperone-like activity of the Rvbs.

Based on our model, we would most simply expect that a hexameric Rvb1/Rvb2 bound to Ino80INS would be created during the ATPase cycle of the Rvbs. While we do observe a small amount of this species upon addition of ATP, we mainly observe Rvb1/Rvb2 hexamers without Ino80INS bound by native MS (Figure 2C). We speculate that the different steps in ATP hydrolysis cause the Rvbs to cycle between strong and weak binding for their client proteins, analogous to other chaperones such as Hsp90 (Street et al., 2011; Verba et al., 2016). In the context of full-length Ino80, additional interactions may keep it bound to the Rvbs during the ATPase cycle, whereas in the context of the Ino80 insert, these additional binding interactions could be missing, causing it to dissociate.

Our model also addresses the potentially separate functions of the hexameric and dodecameric forms of the Rvbs. While both of these oligomeric states been observed in native Rvb1/Rvb2 systems (Ewens et al., 2016; Jeganathan et al., 2015), mechanistic

roles for either oligomeric state have not yet been proposed. We speculate that the dodecameric Rvb1/Rvb2/Ino80INS complex is representative of an intermediate that is on a pathway toward assembling a multi-subunit INO80 complex. Completion of assembly would then result in the stable binding of the less active, hexameric state of Rvb1/Rvb2 to the rest of the INO80 complex. In this model, the transition from dodecamer to hexamer is governed by both the presence of bound client proteins and the ATPase cycle, ultimately resulting in an equilibrium among dodecameric assembly intermediates and fully assembled complexes containing a hexamer of Rvb1/Rvb2. Importantly, the predominant stoichiometry of the components within the Rvb1/Rvb2/Ino80INS complex (6:6:2) is consistent with recently published EM data of the full INO80 complex, where a large number of the INO80 complexes contain a single Ino80 ATPase bound to a hexamer of Rvb1/Rvb2 (Watanabe et al., 2015).

We favor the model described earlier to explain our results, because previous work has suggested that the Rvbs are required for assembly of active INO80 complexes (Chen et al., 2013; Jónsson et al., 2004). However, we propose two alternative models that are also compatible with our results. In the first alternative model, the ATPase stimulation caused by Ino80INS serves to limit the number of Ino80 proteins bound, as increasing the number of bound Ino80 proteins would further destabilize the already metastable dodecamer. In this model, the Rvbs would primarily play a role in regulating subunit stoichiometry. In the second alternative model, the ATPase stimulation caused by Ino80INS may reflect the Rvbs' potential role for remodeling protein complexes, as Rvb1 and Rvb2 have been hypothesized to be involved in disaggregation of amyloid fibrils (Zaarur et al., 2015) and chromosome decondensation (Magalska et al., 2014). Importantly, our observation that protein, not nucleic acid, is a robust activator of Rvb1/Rvb2 helps exclude models involving a helicase-like role of the Rvbs in vivo.

While we believe we have identified the first client of Rvb1/Rvb2, further studies are required to fully demonstrate the chaperone-like potential of the yeast Rvbs. In the future, an ability to reconstitute all the steps in the reaction catalyzed by the Rvbs would be invaluable for obtaining insights into the mechanism of the process. We propose that the yeast INO80 complex can serve as a powerful model system for future mechanistic studies of the Rvbs for the following reasons: (1) the organization and stoichiometry of the INO80 subunits within the native complex, down to residue-level interactions, has been fully characterized (Tosi et al., 2013); and (2) the proper assembly of INO80 is required for in vitro nucleosome remodeling activity (Chen et al., 2013; Jónsson et al., 2001). Thus, the INO80 complex provides an ideal opportunity for a complete in vitro reconstitution of the steps required in assembling an active multi-subunit complex. These experiments, while technically challenging, would provide unprecedented mechanistic insight into this class of essential yet poorly understood AAA+ ATPases.

## EXPERIMENTAL PROCEDURES

Also see [Supplemental Experimental Procedures](#) for additional information.

### Protein Expression and Purification

Rvb1 and Rvb2 were co-expressed in Rosetta (DE3) *E. coli* on a pet28a plasmid (a kind gift from the Hopfner lab). Rvb2 had a TEV (tobacco etch virus)-cleavable N-terminal His<sub>6</sub>-tag, which was cleaved unless otherwise noted. Rvb1/Rvb2 was purified using cobalt affinity resin followed by SEC.

### SEC-MALS

Molecular weight was determined through SEC (using a Wyatt Technology 050S5 SEC column) with an Ettan LC system (GE Healthcare) and in-line DAWN HELEOS MALS system and Optilab T-REX differential refractive index detectors (Wyatt Technology). SEC was performed in 80 mM PIPES (pH 6.9), 150 mM KCl, 5 mM MgCl<sub>2</sub>. Data were analyzed by the ASTRA VI software package (Wyatt Technology).

### XL-MS

Preparations of Rvb1/Rvb2 and Rvb1/Rvb2/Ino80INS were crosslinked with BS3, digested with trypsin, fractionated by SEC, and analyzed by liquid chromatography (LC)-MS using a QExactive Plus mass spectrometer. Spectra were searched for crosslinked peptides using Protein Prospector and were further classified using a support vector machine (SVM) model (Robinson et al., 2015; Trnka et al., 2014).

### Native MS

Native MS was performed on the Rvb1/Rvb2 protein complexes using the Exactive Plus EMR instrument (Thermo Scientific). Samples were buffer exchanged into 150 mM ammonium acetate, pH 7.5, and then sprayed from Au/Pd-coated borosilicate emitters into a mass spectrometer using static infusion.

### Negative-Stain EM

Rvb1/Rvb2/Ino80INS complexes were prepared as described earlier and dialyzed into 25 mM HEPES (pH 7.5), 150 mM KCl. 2.5  $\mu$ L 5–10  $\mu$ M of Rvbs were adsorbed onto 30-s glow-discharged copper grids coated with carbon. Samples were blotted and stained with 3  $\mu$ L 0.75% uranyl formate solution for five applications, with blotting in between each application. Images were collected on a Tecnai T12 microscope (FEI) equipped with a LaB<sub>6</sub> filament and operated at 120 kV. Images were recorded with an Ultrascan 4,096 pixel  $\times$  4,096 pixel charge-coupled device (CCD) camera (Gatan) at a nominal magnification of 52,000 $\times$ .

### ATPases

ATP hydrolysis rates were measured using an NADH enzyme-coupled reaction assay (Lindsley, 2001). The final reaction included 10 U/mL pyruvate kinase (Sigma) and 10 U/mL lactate dehydrogenase (LDH; Sigma), 2 mM phosphoenolpyruvate (PEP; Sigma), between 2 and 10  $\mu$ M Rvb1/2 complex, 0.18 mM NADH, 4 mM ATP, 4.5 mM MgCl<sub>2</sub>, 150 mM KCl, and 25 mM HEPES (pH 7.5). ATP concentration was empirically determined to be saturating for all constructs tested. All components other than Rvb1/2 were assembled and incubated at 30°C in a 384-well plate (clear bottom; Corning) for 10 min. Enzyme was mixed in, and absorbance at 340 nm was monitored using a SpectraMax M5e plate reader. After background subtraction, the data were fit to a linear regression, with the slope being the rate of hydrolysis (micromolar per minute).

### Cryo-EM Image Acquisition

Rvb1/Rvb2/Ino80INS complexes were prepared as described earlier for negative stain. For cryo-EM grid preparation, 2.5  $\mu$ L samples of 10  $\mu$ M Rvb monomer were applied to Quantifoil holey carbon film grids (1.2/1.3 spacing) that had been glow discharged for 30 s. Using a Mark I Vitrobot (FEI), grids were blotted for 5.5 or 6 s with  $-3$  mm offset at 100% humidity and were plunge frozen into liquid ethane cooled by liquid nitrogen.

Images were collected on a Titan Krios microscope (FEI Company), operated at 300 kV under low-dose conditions at the Janelia Research Campus. All images were recorded with a K2 Summit direct electron detector camera (Gatan) using super-resolution counting mode, with a pixel size of 1.31 Å per pixel after 2  $\times$  2 binning for motion correction and subsequent processing. The camera dose rate was set to  $\sim 1.4$  e<sup>-</sup> per pixel per frame.

Dose-fractionated stacks were collected over an exposure time of 8 s with a sub-frame exposure of 200 ms, for a total of 40 subframes, resulting in a total dose of  $\sim 32.6 \text{ e}^-/\text{\AA}^2$  for the entire stack and  $0.8 \text{ e}^-/\text{\AA}$  for each subframe.

### Cryo-EM Image Processing

All dose-fractionated image stacks were motion corrected using MotionCor2, and the sum of all subframes was used for subsequent image processing (Zheng et al., 2017). Estimation of the contrast transfer function (CTF) and defocus was conducted using Gctf, a GPU (graphic processing unit)-accelerated CTF estimation program (Zhang, 2016). A set of  $\sim 1,400$  particles were manually picked and extracted from corrected micrographs using RELION 1.4. Manually picked particles were subjected to 2D classification in RELION 1.4, and good classes were selected as a template for reference-based automatic particle picking. Multiple rounds of 2D classification yielded a particle stack of  $\sim 366,000$  particles that was used to generate a consensus model with the RELION 3D auto-refine function, using C1 symmetry. The structure of the *T. acidophilum* 20S proteasome (EMDB: 5623) filtered to 50 Å was used as an initial model. All subsequent 3D classification was performed using either the consensus model, a model generated by prior 3D classification, or the *C. thermophilum* Rvb1/Rvb2 crystal structure (PDB: 4WVY), all filtered to at least 40 Å, as an initial model. Classes of interest were subjected to further 3D classification with C1 symmetry and refined using gold-standard procedures within RELION 1.4 (Scheres, 2012).

### Integrative Modeling of the Rvb1/Rvb2/Ino80INS Complex

We computed a structural model of the yeast Rvb1/Rvb2/Ino80INS complex using an integrative approach based on data from X-ray crystallography, crosslinking MS, and cryo-EM. The modeling protocol (Figure S6) was scripted using the Python Modeling Interface (PMI), a library for modeling macromolecular complexes based on our open-source Integrative Modeling Platform (IMP) package, v.2.5 (<http://integrativemodeling.org>) (Russel et al., 2012). Complete details of the integrative modeling procedure are in the Supplemental Information. Files containing the input data, scripts, and output structures are available online (<https://github.com/integrativemodeling/Rvbs>).

### ACCESSION NUMBERS

The accession number for the cryo-EM map of the Rvb1/Rvb2/Ino80INS complex reported in this paper is EMDB: 8696.

### SUPPLEMENTAL INFORMATION

Supplemental Information includes Supplemental Experimental Procedures, seven figures, and six tables and can be found with this article online at <http://dx.doi.org/10.1016/j.celrep.2017.05.029>.

### AUTHOR CONTRIBUTIONS

C.Y.Z. conceptualized the study with guidance from G.J.N. C.Y.Z. cloned and purified the proteins and performed ATPase assays and SEC-MALS experiments. J.B.J. performed the native MS experiments. M.J.T. performed the XL-MS experiments, created homology models of Rvb1/Rvb2, and analyzed the data. C.I.S. performed the EM experiments and analyzed the data with help from E.P. I.E. performed the integrative modeling. All authors contributed to the preparation of the manuscript. Y.C., A.S., and A.L.B. provided expertise and support for the project.

### ACKNOWLEDGMENTS

We thank the Hopfner lab (Ludwig-Maximilians University in Munich) for the expression plasmid for the Rvbs. We thank L.R. Pack, S. Coyle, P. Dumesic, L. Hsieh, S. Johnson, A.G. Larson, and D. Canzio for critical reading of the manuscript and members of the Narlikar lab for helpful discussions. We thank D. Elnatan and A. Lyon for technical support. This work was funded by a NIH grant (R01GM073767) to G.J.N.; an NIH Ruth L. Kirschstein National Research Service Award (5F31CA180651-02) to C.Y.Z.; an NSF graduate fellowship

(1144247) to C.I.S.; grants from NIH (8P41GM103481 and 1S10D016229) to A.L.B.; NIH grants (R01GM083960 and P41GM083960) to A.S.; and NIH grants (1S10D020054 and R01GM082893) to Y.C.

Received: April 1, 2016

Revised: April 5, 2017

Accepted: May 9, 2017

Published: June 6, 2017

### REFERENCES

- Alber, F., Dokudovskaya, S., Veenhoff, L.M., Zhang, W., Kipper, J., Devos, D., Suprpto, A., Karni-Schmidt, O., Williams, R., Chait, B.T., et al. (2007). Determining the architectures of macromolecular assemblies. *Nature* **450**, 683–694.
- Chen, L., Conaway, R.C., and Conaway, J.W. (2013). Multiple modes of regulation of the human Ino80 SNF2 ATPase by subunits of the INO80 chromatin-remodeling complex. *Proc. Natl. Acad. Sci. USA* **110**, 20497–20502.
- Cheung, K.L.Y., Huen, J., Kakihara, Y., Houry, W.A., and Ortega, J. (2010). Alternative oligomeric states of the yeast Rvb1/Rvb2 complex induced by histidine tags. *J. Mol. Biol.* **404**, 478–492.
- Ewens, C.A., Su, M., Zhao, L., Nano, N., Houry, W.A., and Southworth, D.R. (2016). Architecture and nucleotide-dependent conformational changes of the Rvb1-Rvb2 AAA+ complex revealed by cryoelectron microscopy. *Structure* **24**, 657–666.
- Gorynia, S., Bandejas, T.M., Pinho, F.G., McVey, C.E., Vornrhein, C., Round, A., Svergun, D.I., Donner, P., Matias, P.M., and Carrondo, M.A. (2011). Structural and functional insights into a dodecameric molecular machine - the RuvBL1/RuvBL2 complex. *J. Struct. Biol.* **176**, 279–291.
- Gribun, A., Cheung, K.L.Y., Huen, J., Ortega, J., and Houry, W.A. (2008). Yeast Rvb1 and Rvb2 are ATP-dependent DNA helicases that form a heterohexameric complex. *J. Mol. Biol.* **376**, 1320–1333.
- Ikura, T., Ogryzko, V.V., Grigoriev, M., Groisman, R., Wang, J., Horikoshi, M., Scully, R., Qin, J., and Nakatani, Y. (2000). Involvement of the TIP60 histone acetylase complex in DNA repair and apoptosis. *Cell* **102**, 463–473.
- Iyer, L.M., Leipe, D.D., Koonin, E.V., and Aravind, L. (2004). Evolutionary history and higher order classification of AAA+ ATPases. *J. Struct. Biol.* **146**, 11–31.
- Izumi, N., Yamashita, A., Iwamatsu, A., Kurata, R., Nakamura, H., Saari, B., Hirano, H., Anderson, P., and Ohno, S. (2010). AAA+ proteins RUVBL1 and RUVBL2 coordinate PIKK activity and function in nonsense-mediated mRNA decay. *Sci. Signal.* **3**, ra27.
- Jeganathan, A., Leong, V., Zhao, L., Huen, J., Nano, N., Houry, W.A., and Ortega, J. (2015). Yeast *rvb1* and *rvb2* proteins oligomerize as a conformationally variable dodecamer with low frequency. *J. Mol. Biol.* **427**, 1875–1886.
- Jónsson, Z.O., Dhar, S.K., Narlikar, G.J., Auty, R., Wagle, N., Pellman, D., Pratt, R.E., Kingston, R., and Dutta, A. (2001). Rvb1p and Rvb2p are essential components of a chromatin remodeling complex that regulates transcription of over 5% of yeast genes. *J. Biol. Chem.* **276**, 16279–16288.
- Jónsson, Z.O., Jha, S., Wohlschlegel, J.A., and Dutta, A. (2004). Rvb1p/Rvb2p recruit Arp5p and assemble a functional Ino80 chromatin remodeling complex. *Mol. Cell* **16**, 465–477.
- Kanemaki, M., Kurokawa, Y., Matsu-ura, T., Makino, Y., Masani, A., Okazaki, K., Morishita, T., and Tamura, T.A. (1999). TIP49b, a new RuvB-like DNA helicase, is included in a complex together with another RuvB-like DNA helicase, TIP49a. *J. Biol. Chem.* **274**, 22437–22444.
- Kim, M. (2013). Beta conformation of polyglutamine track revealed by a crystal structure of Huntingtin N-terminal region with insertion of three histidine residues. *Prion* **7**, 221–228.
- Lakomek, K., Stoehr, G., Tosi, A., Schmailzl, M., and Hopfner, K.-P. (2015). Structural basis for dodecameric assembly states and conformational plasticity of the full-length AAA+ ATPases Rvb1 · Rvb2. *Structure* **23**, 483–495.
- Leitner, A., Faini, M., Stengel, F., and Aebersold, R. (2016). Crosslinking and mass spectrometry: an integrated technology to understand the structure and function of molecular machines. *Trends Biochem. Sci.* **41**, 20–32.

- Lindsley, J.E. (2001). Use of a real-time, coupled assay to measure the ATPase activity of DNA topoisomerase II. *Methods Mol. Biol.* **95**, 57–64.
- López-Perrote, A., Muñoz-Hernández, H., Gil, D., and Llorca, O. (2012). Conformational transitions regulate the exposure of a DNA-binding domain in the RuvBL1-RuvBL2 complex. *Nucleic Acids Res.* **40**, 11086–11099.
- Magalska, A., Schellhaus, A.K., Moreno-Andrés, D., Zanini, F., Schooley, A., Sachdev, R., Schwarz, H., Madlung, J., and Antonin, W. (2014). RuvB-like ATPases function in chromatin decondensation at the end of mitosis. *Dev. Cell* **31**, 305–318.
- Makino, Y., Kanemaki, M., Kurokawa, Y., Koji, T., and Tamura, Ta. (1999). A rat RuvB-like protein, TIP49a, is a germ cell-enriched novel DNA helicase. *J. Biol. Chem.* **274**, 15329–15335.
- Matias, P.M., Baek, S.H., Bandejas, T.M., Dutta, A., Houry, W.A., Llorca, O., and Rosenbaum, J. (2015). The AAA+ proteins Pontin and Reptin enter adult age: from understanding their basic biology to the identification of selective inhibitors. *Front. Mol. Biosci.* **2**, 17.
- Matias, P.M., Gorynia, S., Donner, P., and Carrondo, M.A. (2006). Crystal structure of the human AAA+ protein RuvBL1. *J. Biol. Chem.* **281**, 38918–38929.
- McKeegan, K.S., Debieux, C.M., and Watkins, N.J. (2009). Evidence that the AAA+ proteins TIP48 and TIP49 bridge interactions between 15.5K and the related NOP56 and NOP58 proteins during box C/D snoRNP biogenesis. *Mol. Cell. Biol.* **29**, 4971–4981.
- Nano, N., and Houry, W.A. (2013). Chaperone-like activity of the AAA+ proteins Rvb1 and Rvb2 in the assembly of various complexes. *Philos. Trans. R. Soc. Lond. B Biol. Sci.* **368**, 20110399.
- Niewiarowski, A., Bradley, A.S., Gor, J., McKay, A.R., Perkins, S.J., and Tsaneva, I.R. (2010). Oligomeric assembly and interactions within the human RuvB-like RuvBL1 and RuvBL2 complexes. *Biochem. J.* **429**, 113–125.
- Petukhov, M., Dagkessamanskaja, A., Bommer, M., Barrett, T., Tsaneva, I., Yakimov, A., Quéval, R., Shvetsov, A., Khodorkovskiy, M., Käs, E., and Grigoriev, M. (2012). Large-scale conformational flexibility determines the properties of AAA+ TIP49 ATPases. *Structure* **20**, 1321–1331.
- Puri, T., Wandler, P., Sigala, B., Saibil, H., and Tsaneva, I.R. (2007). Dodecameric structure and ATPase activity of the human TIP48/TIP49 complex. *J. Mol. Biol.* **366**, 179–192.
- Qiu, X.B., Lin, Y.L., Thome, K.C., Pian, P., Schlegel, B.P., Weremowicz, S., Parvin, J.D., and Dutta, A. (1998). An eukaryotic RuvB-like protein (RUVBL1) essential for growth. *J. Biol. Chem.* **273**, 27786–27793.
- Robinson, P.J., Trnka, M.J., Pellarin, R., Greenberg, C.H., Bushnell, D.A., Davis, R., Burlingame, A.L., Sali, A., and Kornberg, R.D. (2015). Molecular architecture of the yeast Mediator complex. *eLife* **4**, 08719.
- Rose, R.J., Damoc, E., Denisov, E., Makarov, A., and Heck, A.J.R. (2012). High-sensitivity Orbitrap mass analysis of intact macromolecular assemblies. *Nat. Methods* **9**, 1084–1086.
- Russel, D., Lasker, K., Webb, B., Velázquez-Muriel, J., Tjioe, E., Schneidman-Duhovny, D., Peterson, B., and Sali, A. (2012). Putting the pieces together: integrative modeling platform software for structure determination of macromolecular assemblies. *PLoS Biol.* **10**, e1001244.
- Scheres, S.H.W. (2012). RELION: implementation of a Bayesian approach to cryo-EM structure determination. *J. Struct. Biol.* **180**, 519–530.
- Shi, Y., Fernandez-Martinez, J., Tjioe, E., Pellarin, R., Kim, S.J., Williams, R., Schneidman-Duhovny, D., Sali, A., Rout, M.P., and Chait, B.T. (2014). Structural characterization by cross-linking reveals the detailed architecture of a coatmer-related heptameric module from the nuclear pore complex. *Mol. Cell. Proteomics* **13**, 2927–2943.
- Silva-Martin, N., Daudén, M.I., Glatt, S., Hoffmann, N.A., Kastiris, P., Bork, P., Beck, M., and Müller, C.W. (2016). The combination of X-ray crystallography and cryo-electron microscopy provides insight into the overall architecture of the dodecameric Rvb1/Rvb2 complex. *PLoS ONE* **11**, e0146457.
- Singleton, M.R., Dillingham, M.S., and Wigley, D.B. (2007). Structure and mechanism of helicases and nucleic acid translocases. *Annu. Rev. Biochem.* **76**, 23–50.
- Street, T.O., Lavery, L.A., and Agard, D.A. (2011). Substrate binding drives large-scale conformational changes in the Hsp90 molecular chaperone. *Mol. Cell* **42**, 96–105.
- Tosi, A., Haas, C., Herzog, F., Gilmozzi, A., Berninghausen, O., Ungewickell, C., Gerhold, C.B., Lakomek, K., Aebersold, R., Beckmann, R., and Hopfner, K.-P. (2013). Structure and subunit topology of the INO80 chromatin remodeler and its nucleosome complex. *Cell* **154**, 1207–1219.
- Trnka, M.J., Baker, P.R., Robinson, P.J., Burlingame, A.L., and Chalkley, R.J. (2014). Matching cross-linked peptide spectra: only as good as the worse identification. *Mol. Cell. Proteomics* **13**, 420–434.
- Venteicher, A.S., Meng, Z., Mason, P.J., Veenstra, T.D., and Artandi, S.E. (2008). Identification of ATPases pontin and reptin as telomerase components essential for holoenzyme assembly. *Cell* **132**, 945–957.
- Verba, K.A., Wang, R.Y.-R., Arakawa, A., Liu, Y., Shirouzu, M., Yokoyama, S., and Agard, D.A. (2016). Atomic structure of Hsp90-Cdc37-Cdk4 reveals that Hsp90 traps and stabilizes an unfolded kinase. *Science* **352**, 1542–1547.
- Watanabe, S., Tan, D., Lakshminarasimhan, M., Washburn, M.P., Hong, E.J., Walz, T., and Peterson, C.L. (2015). Structural analyses of the chromatin remodelling enzymes INO80-C and SWR-C. *Nat. Commun.* **6**, 7108.
- White, S.R., and Lauring, B. (2007). AAA+ ATPases: achieving diversity of function with conserved machinery. *Traffic* **8**, 1657–1667.
- Zaarur, N., Xu, X., Lestienne, P., Meriin, A.B., McComb, M., Costello, C.E., Newnam, G.P., Ganti, R., Romanova, N.V., Shanmugasundaram, M., et al. (2015). RuvbL1 and RuvbL2 enhance aggresome formation and disaggregate amyloid fibrils. *EMBO J.* **34**, 2363–2382.
- Zhang, K. (2016). Gctf: Real-time CTF determination and correction. *J. Struct. Biol.* **193**, 1–12.
- Zheng, S.Q., Palovcak, E., Armache, J.-P., Verba, K.A., Cheng, Y., and Agard, D.A. (2017). MotionCor2: anisotropic correction of beam-induced motion for improved cryo-electron microscopy. *Nat. Methods* **14**, 331–332.